

Continuum descriptions of spatial spreading for heterogeneous cell populations: theory and experiment

Oleksii M Matsiaka¹, Ruth E Baker², *Matthew J Simpson¹

¹ *School of Mathematical Sciences, Queensland University of Technology (QUT)
Brisbane, Queensland, Australia.*

² *Mathematical Institute, University of Oxford, Radcliffe Observatory Quarter,
Woodstock Road, Oxford, United Kingdom.*

Abstract

Variability in cell populations is frequently observed in both *in vitro* and *in vivo* settings. Intrinsic differences within populations of cells, such as differences in cell sizes or differences in rates of cell motility, can be present even within a population of cells from the same cell line. We refer to this variability as cell *heterogeneity*. Mathematical models of cell migration, for example, in the context of tumour growth and metastatic invasion, often account for both undirected (random) migration and directed migration that is mediated by cell-to-cell contacts and cell-to-cell adhesion. A key feature of standard models is that they often assume that the population is composed of identical cells with constant properties. This leads to relatively simple single-species *homogeneous* models that neglect the role of heterogeneity. In this work, we use a continuum modelling approach to explore the role of heterogeneity in spatial spreading of cell populations. We employ a three-species heterogeneous model of cell motility that explicitly incorporates different types of experimentally-

motivated heterogeneity in cell sizes: (i) monotonically decreasing; (ii) uniform; (iii) non-monotonic; and (iv) monotonically increasing distributions of cell size. Comparing the density profiles generated by the three-species heterogeneous model with density profiles predicted by a more standard single-species homogeneous model reveals that when we are dealing with some forms of heterogeneity a simple and computationally efficient single-species homogeneous model can be remarkably accurate in describing the evolution of a heterogeneous cell population. In contrast, we also identify other forms of heterogeneity for which the simpler single-species homogeneous model performs relatively poorly. Additional results for heterogeneity in parameters describing both undirected and directed cell migration are also considered, and we find that similar results apply.

Key words: Cell migration; heterogeneity; continuum description; scratch assay

* Corresponding author

Email address: matthew.simpson@qut.edu.au, *Telephone* + 617 31385241, *Fax* + 617 3138 2310 (*Matthew J Simpson¹).

1 Introduction

2 *In vitro* cell migration experiments play an important role in the discovery and
3 testing of putative drug treatments, the study of malignant tumour growth
4 and metastasis, as well as tissue regeneration and repair (Savla et al., 2004;
5 Sengers et al., 2007; Tremel et al., 2009; Sarapata and de Pillis, 2010; Ger-
6 lee, 2013; Edmondson et al., 2014; Shah et al., 2016). Mathematical models
7 of many biological processes involved in these experiments normally require
8 certain assumptions to make the problem mathematically and computation-
9 ally tractable. When modelling large populations of cells, one of the most
10 intuitive approaches is to assume that all cells have fixed properties, such
11 as assuming all cells have constant size and constant diffusivity (Sherratt
12 and Murray, 1990; Galle et al., 2005; Simpson et al., 2013). In this frame-
13 work a cell population is considered to be a *homogeneous* population, and
14 single-species homogeneous models are routinely invoked (Maini et al., 2004a;
15 Maini et al., 2004b; Sepulveda et al., 2013; Simpson et al., 2013; George et
16 al., 2017). Single-species homogeneous models are much less computationally
17 expensive than more elaborate multi-species heterogeneous models and, as a
18 result, are frequently used relative to multi-species counterparts. In addition,
19 multi-species frameworks usually involve a significantly larger number of free
20 model parameters that we may have little prior knowledge about and so the
21 process of calibrating multi-species heterogeneous models to match experimen-
22 tal observations is significantly more challenging than calibrating single-species
23 homogeneous models. This is an important consideration because it is well-
24 known that parameterising mathematical models of biological processes can
25 be challenging, often requiring computationally-intensive methods (Pozzobon

26 and Perré, 2018; Warne et al. 2019).

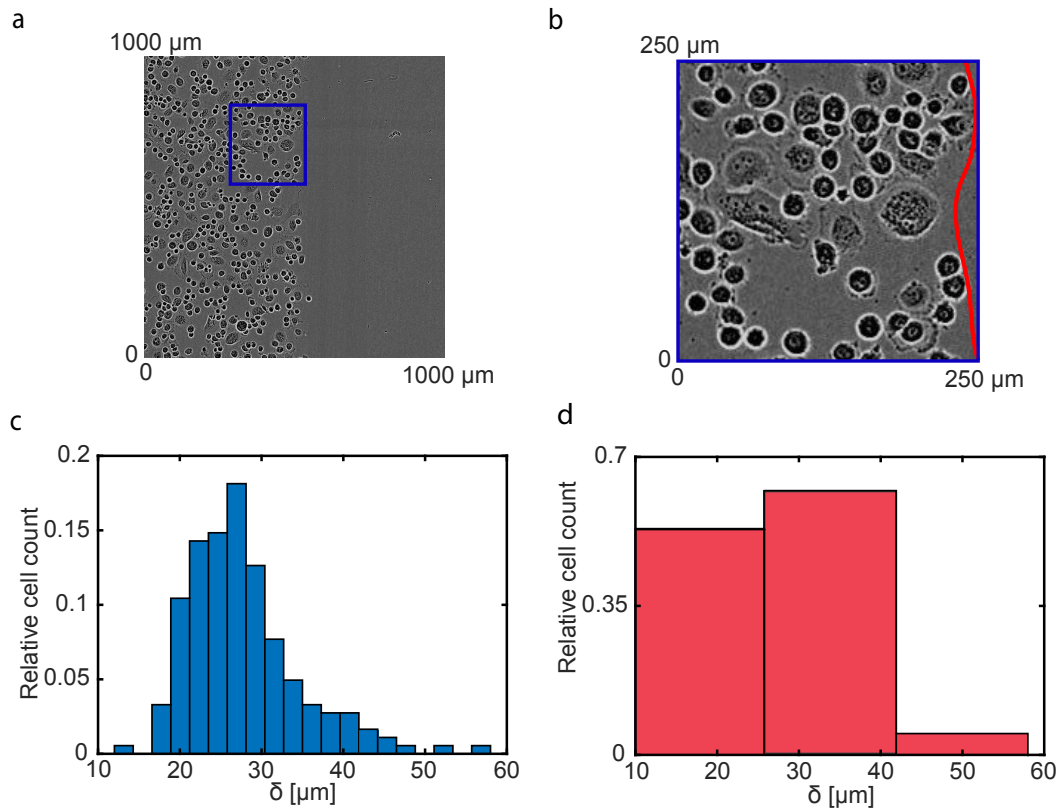


Fig. 1. Heterogeneity in a population of PC-3 prostate cancer cells (Kaighn et al., 1979). (a) Experimental image of an advancing cell population and corresponding cell size distribution. The red solid line denotes position of the leading edge. (b) Detailed image of the subregion denoted in the blue rectangle in Figure 1(a). (c) Cell size distribution with a bin size of $15 \mu\text{m}$. The cell size distribution is obtained from the sample of 184 cells randomly selected from the population. (d) Cell size distribution with a bin size of $2.3 \mu\text{m}$. The histogram in Figure 1(d) is constructed using the same sample of 184 cells.

27 Although *heterogeneity* in cell populations is frequently observed in experi-
28 ments, there is relatively little guidance or consensus in the literature about
29 how to incorporate such heterogeneity into the mathematical models used
30 to replicate and predict such experiments (An et al., 2001; Altschuler et al.,
31 2010). Figure 1(a)-(b) shows a typical experiment where we can clearly vi-
32 sually observe cells of different sizes. The measured cell size distribution in
33 Figure 1(c) quantifies this heterogeneity in cell sizes and raises the question if

34 the most straightforward approach of applying a single-species homogeneous
35 model can be reasonably used to predict the spatial spreading of this clearly
36 heterogeneous population. In addition to the clear visual heterogeneity in cell
37 sizes, it could be relevant to consider that cells of different sizes can exhibit
38 different behaviour such as different rates of motility, or different mechani-
39 cal properties including resistance to deformation and adhesion. Therefore,
40 it could be possible that there are multiple types of heterogeneity acting in
41 even this very simple experiment. Previously, heterogeneity in cell populations
42 has been introduced in both discrete and continuum models of cell motility
43 (Simpson et al., 2014; Jin et al., 2016b; Sundstrom et al., 2016; Matsiaka et
44 al., 2017). However, these previous modelling studies do not address the basic
45 question of identifying whether it is absolutely necessary to apply a multi-
46 species heterogeneous models to obtain a faithful description of the behaviour
47 of the heterogeneous population and whether different forms of heterogeneity
48 affect the answer to this fundamental question.

49 In our work we use an experimentally-motivated approach to investigate the
50 role of heterogeneity in two-dimensional scratch assays, and we compare the
51 performance of a single-species homogeneous model relative to a heteroge-
52 neous multi-species model. We use numerical solutions of the multi-species
53 heterogeneous model to produce synthetic test data that we use to investigate
54 the performance of a simpler single-species homogeneous model. To mimic
55 experimental data, such as depicted in Figure 1, we use the multi-species
56 continuum approach introduced by Matsiaka et al. (2017). To keep our work
57 tractable, we describe the heterogeneity by dividing the total population into
58 three subpopulations with varying properties. The choice of working with three
59 subpopulations allows us to keep the model computationally tractable while

60 capturing important differences in the population properties, as illustrated
61 in Figure 1(d). Throughout this work we consider four distinct distributions
62 of cell sizes: (i) monotonically decreasing; (ii) uniform; (iii) non-monotonic;
63 and (iv) monotonically increasing distributions of cell size. The monotonically
64 decreasing distribution, as shown in Figure 3(a), is a fairly accurate approxi-
65 mation of the experimentally observed cell size distribution in Figure 1(d). The
66 other three kinds of distributions are included in our work for completeness.
67 Our findings suggest that, for certain cell size distributions, namely monoton-
68 ically decreasing and uniform distributions, the single-species homogeneous
69 model performs remarkably well with an excellent match between the den-
70 sity profiles generated by the three-species heterogeneous model and density
71 profiles predicted by its single-species homogeneous analogue. Therefore, our
72 results imply that applying a single-species homogeneous model to describe
73 experiments with monotonically decreasing or uniform cell size distributions
74 might be sufficient for accurately predicting population-level behaviour. In
75 contrast, the data with non-monotonic and monotonically increasing cell size
76 distributions might require the application of multi-species models to account
77 for differences in population.

78 This manuscript is organised in the following way. In Section 2 we describe
79 experimental data for a series of two-dimensional scratch assays that clearly
80 involve a significant level of heterogeneity among the population. In Section 3
81 we introduce a mathematical model of the cell motility and adhesion. In partic-
82 ular, we focus on two analogues of the mathematical model: (i) a three-species
83 heterogeneous model of cell motility where parameters including cell size, cell
84 diffusivity and cell adhesion strength can vary between the subpopulations;
85 and (ii) a more traditional single-species homogeneous model of cell motility

86 where all cells in the population are treated as having the same cell size, cell
87 diffusivity and cell adhesion strength. Results in Section 4 compare perfor-
88 mance of the single-species homogeneous model as applied to data generated
89 using the three-species heterogeneous model for different cell size distributions.
90 Additional results exploring the role of heterogeneity in both the undirected
91 (diffusive) and directed (adhesion/cell-to-cell contacts) migration are detailed
92 in the Supplementary Material. Finally, in Section 5 we summarise our result
93 and propose potential extensions.

94 **2 Experimental data**

95 Monolayer scratch assays are performed using the IncuCyte ZOOMTM sys-
96 tem (Essen BioScience). In all experiments we use the PC-3 prostate cancer
97 cell line (Kaighn et al., 1979) from the American Type Culture Collection
98 (ATCCTM, Manassas, USA). After growing, cells are removed from the flask
99 using TrypLETM (ThermoFisher Scientific) in phosphate buffered saline, re-
100 suspended in growth medium and seeded at a density of 20,000 cells per well in
101 96-well ImageLock plates (Essen BioScience). The diameter of each individual
102 well is 9000 μm .

103 Mitomycin-C is added at a concentration of 10 $\mu\text{g}/\text{mL}$ for two hours before a
104 scratch is made in the monolayer of cells (Sadeghi et al., 1998). Mitomycin-C
105 is a chemotherapy drug that blocks DNA replication and, consequently, stops
106 proliferation. As a result of treatment the number of cells in the assay remains
107 approximately constant since cells neither proliferate or die on the timescale of
108 the experiment. Often scratch assays are performed using mitomycin-C treated
109 cells so that the experiment focuses only upon the role of cell migration as

110 opposed to the combined effects of cell migration and cell proliferation. A
111 WoundMakerTM (Essen BioScience) is used to create identical scratches in
112 the uniformly distributed populations. Medium is aspirated after scratching;
113 each well is washed twice and refilled with fresh medium (100 μ L). Plates are
114 incubated in the IncuCyte ZOOMTM and photographed every two hours for
115 48 hours. In total, these experiments are performed in eight of the 96 wells
116 on the 96-well plate. In our work we use one of the experimental replicates at
117 $t = 0$ h, Figure 1, to quantify the heterogeneity in a cell population.

118 To quantify the heterogeneity in cell size we randomly select 184 cells from
119 the experimental image in Figure 1(a) at $t = 0$ h. Assuming each cell can be
120 treated as a disc, we estimate the equivalent diameter of each individual cell
121 using the following approach. First, we use the histogram tool in Photoshop
122 CS5 to count a number of pixels in the area occupied by each individual cell.
123 The pixel count is converted to an area, A . Second, we estimate the equivalent
124 diameter, $\delta = \sqrt{4A/\pi}$ and use this data to produce histograms to illustrate
125 and visualise the variability in cell size within the experiment. The result-
126 ing cell size distribution, presented as a histogram constructed with bin width
127 $2.3 \mu\text{m}$, is shown in Figure 1(d). The bin width $2.3 \mu\text{m}$ is chosen to demonstrate
128 the fine structure within the cell population that is not normally incorporated
129 in mathematical models of cell migration. However, the computational sim-
130 ulation of a population with the cell size distribution shown in Figure 1(c)
131 is impractical since it would require significant computational resources to
132 simulate the dynamics of 17 distinct subpopulations. As a compromise, we
133 increase the bin width to reduce the number of distinct subpopulations while
134 still retaining a sufficient number of bins to allow us to broadly characterise
135 the heterogeneity in the population. Figure 1(d) demonstrates the histogram

136 of cell sizes constructed using the same sample of cells with a larger bin size
137 width of $15\ \mu\text{m}$. Here, we have three subpopulations that capture the key
138 trends in the heterogeneity in Figure 1(c) without needing to deal with 17
139 distinct subpopulations.

140 **3 Mathematical model**

141 Discrete, stochastic models are often used to describe the spatial spreading of
142 a population of cells, especially when the population of cells is not too large.
143 Here, cells move and interact with each other via predefined force function, as
144 illustrated schematically in Figure 2 (Newman and Grima, 2004; Callaghan et
145 al., 2006; Hasenauer et al., 2011; Frascoli et al. 2013; Osborne et al., 2017).
146 This approach is *individual based* in the sense that knowledge about the move-
147 ment of each individual is essential to infer the evolution of a density on the
148 population-level scale. One of the most popular individual based modelling
149 approaches makes the assumption that the motion of each cell can be de-
150 scribed by a Langevin stochastic differential equation (Newman and Grima,
151 2004; Middleton et al., 2014). As such, the system of N cells is described by
152 a system of N stochastic differential equations of the form

$$\frac{d\vec{x}_i}{dt} = \sum_{i \neq j} \vec{F}_{ij} + \vec{\xi}_i, \quad (3.1)$$

153 where \vec{x}_i is the position vector of the i th cell, \vec{F}_{ij} is the interaction force be-
154 tween cells i and j , and $\vec{\xi}_i$ is the random stochastic force acting upon cell i
155 (Middleton et al., 2014; George et al., 2017; Osborne et al., 2017). The interac-
156 tion force, \vec{F}_{ij} , can be used to parametrise various features of cell populations,

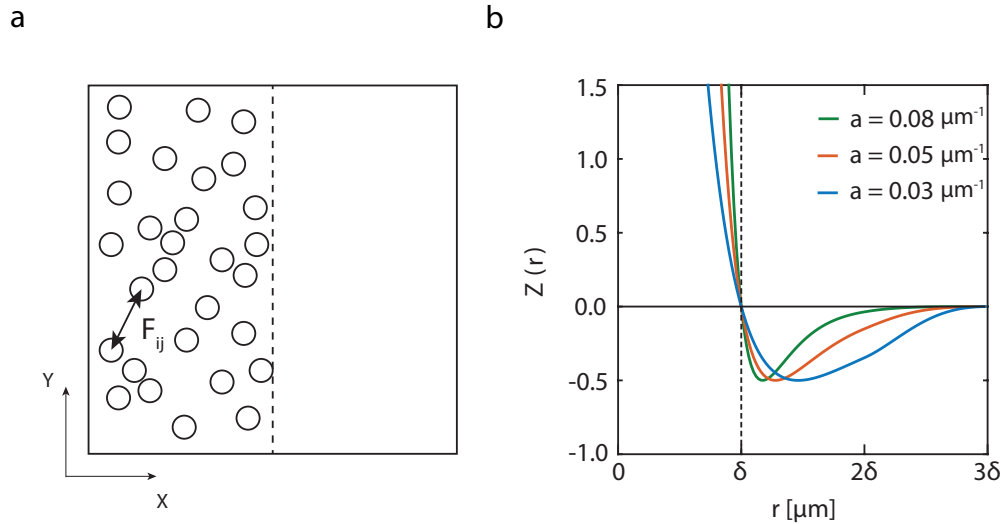


Fig. 2. (a) An idealisation of the front-like distribution of cells in the experimental design shown in Figure 1(a). Here all cells are of constant size. F_{ij} is the interaction force between cell i and cell j . The vertical dashed line represents the approximate leading edge of the population. (b) A typical cell-to-cell interaction force function in the form of the modified Morse potential, $Z(r)$, (Equation (3.7)) used to mimic adhesion and repulsion between individual cells. The vertical dashed line represents the diameter of individual agents, δ . The horizontal line at $Z(r) = 0$ shows the change from long-range attraction ($Z(r) < 0$ for $r > \delta$) to short-range repulsion ($Z(r) > 0$ for $r < \delta$).

157 including heterogeneity. In fact, it is relatively straightforward to model het-
 158 erogeneity in cell sizes in a discrete framework since the interaction force, \vec{F}_{ij} ,
 159 can be chosen to explicitly include the cell size as a parameter (Matsiaka et al.,
 160 2018). Here we can easily differentiate the population into an arbitrary num-
 161 ber of subpopulations by assigning the value of the cell size to each member of
 162 the population. Despite the many advantages of this kind of individual based
 163 modelling approach, such individual based models are computationally inef-
 164 ficient as the number of cells, N , increases. This is because the computation
 165 time required to simulate such models increases with N .

166 In contrast, continuum models based on partial differential equations (PDEs)
 167 are much more convenient to model large cell populations because the time

168 taken to solve continuum PDE models is independent of the size of the pop-
169 ulation (Sherratt and Murray, 1990; Sheardown and Cheng, 1995; Cai et al.,
170 2007; Wise et al., 2008). Often, PDE models are derived using continuum-limit
171 approximations of underlying discrete models and are able to retain certain
172 features of discrete (Middleton et al., 2014; O’Dea and King, 2012). In this
173 work we focus on a continuum model that is derived by taking the limit of
174 a three-species heterogeneous individual based model (Matsiaka et al., 2017).
175 This approach allows us to conceptually incorporate key features of the hetero-
176 geneous cell populations into a discrete modelling framework, and then using
177 a computationally efficient approach to solve the resulting continuum-limit
178 PDE description of the underlying heterogeneous model.

179 We note that, due to the geometry of experiments presented in Figure 1, we
180 are interested in the net movement of cells in only one direction, in this case
181 the horizontal direction (Jin et al., 2016a). This is due to the fact that the
182 net flux of cells in the vertical direction is, on average, zero because of the
183 symmetry in the initial conditions of a scratch assay. Consequently, we focus
184 on a one-dimensional continuum model and consider the evolution of the total
185 cell population in the horizontal direction only. The use of a one-dimensional
186 framework to describe two-dimensional scratch assays has been previously
187 demonstrated to be a convenient approach to reduce the computational com-
188 plexity while still describing the key features of the experiment (Matsiaka et
189 al., 2018).

190 Here we employ a mean field model describing the spatial spreading of a pop-
191 ulation of cells composed of three distinct subpopulations. In one-dimension,

192 the model can be written as

$$\frac{\partial p^{(1)}(x, t)}{\partial t} = D_1 \Delta p^{(1)}(x, t) + \nabla(p^{(1)}(x, t) V^{(1,1)}(x, t)) - \sum_{m=1}^3 n_m \nabla(p^{(1)}(x, t) V^{(1,m)}(x, t)), \quad (3.2)$$

$$\frac{\partial p^{(2)}(x, t)}{\partial t} = D_2 \Delta p^{(2)}(x, t) + \nabla(p^{(2)}(x, t) V^{(2,2)}(x, t)) - \sum_{m=1}^3 n_m \nabla(p^{(2)}(x, t) V^{(2,m)}(x, t)), \quad (3.3)$$

$$\frac{\partial p^{(3)}(x, t)}{\partial t} = D_3 \Delta p^{(3)}(x, t) + \nabla(p^{(3)}(x, t) V^{(3,3)}(x, t)) - \sum_{m=1}^3 n_m \nabla(p^{(3)}(x, t) V^{(3,m)}(x, t)), \quad (3.4)$$

$$V^{(l,m)}(x, t) = \int_{\Omega} F^{(l,m)}(x - y) p^{(m)}(y, t) dy, \quad (3.5)$$

193 where $p^{(1)}(x, t)$, $p^{(2)}(x, t)$, and $p^{(3)}(x, t)$ are the cell densities associated with
 194 each subpopulation and depend on position x and time t . In this heterogeneous
 195 model, D_1 , D_2 , and D_3 are diffusivities of subpopulations 1, 2, and 3, n_1 , n_2 ,
 196 and n_3 are the numbers of cells in each subpopulation, and $V^{(l,m)}(x, t)$ is the
 197 velocity field of subpopulation l induced by subpopulation m (Matsiaka et
 198 al., 2017). The diffusivity constants parameterise the undirected migration of
 199 each subpopulation and the velocity fields describe the directed migration of
 200 each subpopulation that is driven by a combination of cell-to-cell adhesion
 201 and crowding effects.

202 The interaction force between subpopulations l and m that describes directed
 203 migration is given by

$$F^{(l,m)}(x - y) = f_0 \mathcal{Z}(r) \operatorname{sgn}(x - y), \quad (3.6)$$

204 where f_0 is the dimensional amplitude of the interaction force, $\mathcal{Z}(r)$ is a di-

205 dimensionless function that parametrises different features of the cell-to-cell in-
206 teractions, and sgn is the signum function. We choose to include long-range
207 attraction that models cell-to-cell adhesion, and a short-range repulsion that
208 reflects volume exclusion effects (Frascoli et al., 2013). A number of different
209 phenomenological laws, $\mathcal{Z}(r)$, are used to model repulsive and adhesive inter-
210 cellular forces (Murray et al., 2009; Jeon et al., 2010; Middleton et al., 2014).
211 In our work we adopt modified Morse potential in the form

$$\mathcal{Z}(r) = \begin{cases} 2\left(\exp[-2a(r-\delta)] - \exp[-a(r-\delta)]\right), & r < 2\delta, \\ 2\left(\exp[-2a(r-\delta)] - \exp[-a(r-\delta)]\right)g(r), & 2\delta \leq r \leq 3\delta, \\ 0, & r > 3\delta, \end{cases} \quad (3.7)$$

212 where a is the shape parameter that controls the shape of the force func-
213 tion, δ is the cell size, and $r = |x - y|$. We fix the value of the shape
214 parameter at $a = 0.08 \mu\text{m}^{-1}$ (Matsiaka et al., 2017). The function $g(r) =$
215 $\left(1 - \sin\left[(2\pi r - \pi\delta)/2\delta\right]\right)/2$ is the Tersoff cut-off function introduced to im-
216 pose a finite range of intercellular interactions (Tersoff, 1988). A sketch of
217 the potential function given by Equation (3.7) for different values of the pa-
218 rameter a is shown in Figure 2(b) confirming that this potential function
219 describes short range repulsion, longer range attraction and no interactions at
220 over much longer distances. In summary, the key parameters in our model are:
221 (i) cell size, δ ; (ii) the cell diffusivity, D ; and (iii) the amplitude of interaction
222 forces, f_0 . In this work we will systematically explore how heterogeneity in
223 each of these three key parameters influences whether we need to consider a
224 complex heterogeneous multi-species model or whether we can describe the
225 spatial spreading of a cell population using a relatively simple homogeneous,
226 single-species models. Since our experimental data in Figure 1 allows us to

227 explicitly characterise the heterogeneity in cell size, all results in the main
228 document focus on cell size. Additional results in the Supplementary Material
229 focus on heterogeneity in D and f_0 to provide additional insight into the role
230 of heterogeneity in these kinds of experiments.

231 We define the total density of the heterogeneous population as

$$\mathcal{P}(x, t) = \sum_{i=1}^3 \left[p^{(i)}(x, t) \right], \quad (3.8)$$

232 where $p^{(i)}(x, t)$ is the cell density of subpopulation $i = 1, 2, 3$ predicted by
233 Equations (3.2)-(3.4), and $\mathcal{P}(x, t)$ is the total cell density. It is important to
234 interpret the solutions of Equations (3.2)-(3.4) in terms of total cell density
235 since standard experimental protocols do not normally facilitate the measure-
236 ment of spatial and temporal distributions of various subpopulations (Cai et
237 al., 2007; Treloar et al., 2014).

238 We can reduce the three-species heterogeneous system of equations, Equations
239 (3.2)-(3.4), to obtain a single-species homogeneous model in the form,

$$\frac{\partial P(x, t)}{\partial t} = D\Delta P(x, t) - (N - 1)\nabla \left(P(x, t) V(x, t) \right), \quad (3.9)$$

240 where $P(x, t)$ is the cell density of the total population, $N = \sum_{i=1}^3 n_i$ is the
241 total number of cells in the population. Here we assume that the cell size, dif-
242 fusivity and strength of the interaction force for each population is constant,
243 giving $\delta_i = \delta$ and $D_i = D$ for $i = 1, 2, 3$ with f_0 also being treated as a constant
244 across the population. The key differences between the homogeneous single-
245 species model, Equation (3.9), and the three-species heterogeneous model,
246 Equations (3.2)-(3.4) are: (i) the three-species heterogeneous model incorpo-

247 rates three advection-diffusion equations while the single-species homogeneous
248 model is given by a single advection-diffusion equation; (ii) the three-species
249 heterogeneous model contains up to nine free parameters as opposed to three
250 parameters in the single-species homogeneous model.

251 The initial conditions in all simulations are chosen to mimic a cell front, such
252 as that shown in our experimental data set, Figure 1(a). As such, we adopt
253 an initial cell distribution in the form of the one-dimensional step function,

$$P(x, 0) = \mathcal{P}(x, 0) = \begin{cases} 23.9 \times 10^{-3} \text{ cells}/\mu\text{m}, & 0 \mu\text{m} < x < 1000 \mu\text{m}, \\ 0 & \text{cells}/\mu\text{m}, \quad 1000 \mu\text{m} < x < 2000 \mu\text{m}, \end{cases} \quad (3.10)$$

254 on $0 < x < 2000 \mu\text{m}$, which is consistent with a length-scale of a typical *in*
255 *vitro* experiment (Jin et al., 2016a). The initial cell distribution in the hetero-
256 geneous model is given by the sum of initial densities of three subpopulations,
257 $\mathcal{P}(x, 0) = \sum_i p^{(i)}(x, 0)$, where the density of each subpopulation, $p^{(i)}(x, 0)$,
258 varies between each cell size distribution and can be inferred from the his-
259 tograms in Figure 3(a). The value of the initial density of the total population
260 is chosen to represent fairly confluent population of cells. For example, the
261 simulation of the three-species population with the monotonically decreasing
262 cell size distribution, Set Ia, is initiated with the confluence level of approx-
263 imately 65% of maximum packing density, which is fairly typical for scratch
264 assay experiments (Jin et al., 2016; Matsiaka et al., 2017). We note that the
265 boundary of the experimental image in Figure 1(a) is not a physical boundary
266 and cells can freely move across this boundary because the image captures
267 only a small fraction of a much larger experimental domain (Simpson et al.,
268 2018). During the experiment, cells freely migrate, in each direction, across

269 the boundary. However, since the density of cells away from the scratch is
270 spatially uniform, the net flux of cells across the boundary of the image is
271 zero. To capture this situation we impose zero net flux boundary conditions
272 at $x = 0 \mu\text{m}$ and $x = 2000 \mu\text{m}$.

273 All continuum results for single-species homogeneous and three-species het-
274 erogeneous models, given by Equation (3.9) and Equations (3.2)-(3.4), respec-
275 tively, are solved numerically using the method of lines with $\Delta x = 4 \mu\text{m}$ and
276 $\Delta t = 0.005 \text{ h}$ on $0 < x < 2000 \mu\text{m}$ (Matsiaka et al., 2017). We find that this
277 choice of spatial and temporal discretisations are sufficiently fine to produce
278 grid independent results. The detailed discretisation scheme used in this work
279 is presented in the Supplementary material.

280 4 Results and Discussion

281 To investigate the ability of a single-species homogeneous model to capture
282 the behaviour of the three-species heterogeneous analogue, we consider a series
283 of case studies. In these case studies we vary only one parameter at a time to
284 simplify our analysis and to focus on the impact of each individual parame-
285 ter. Another approach would be to use the mathematical models to explore
286 heterogeneity multiple parameter at the same time. However, in this first in-
287 stance, we prefer to take a more fundamental approach and examine the role
288 of heterogeneity in each parameter separately. In the first set of experiments,
289 Set I, we vary the cell size, δ , while keeping D and f_0 fixed at $D = 250 \mu\text{m}^2/\text{h}$
290 and $f_0 = 1.0 \mu\text{m}/\text{h}$, respectively (Matsiaka et al., 2019). These estimates of D
291 and f_0 are based on detailed experimental measurements reported previously
292 (Matsiaka et al., 2019).

293 There are number of ways to quantify performance of the single-species ho-
294 mogeneous model in our framework. The position of the leading edge of the
295 spreading population is routinely used by experimentalists to provide quanti-
296 tative insights into the rate of spatial spreading of a cell population (Treloar
297 and Simpson, 2013; Johnston et al., 2014; Nardini et al., 2016; Bobadilla et
298 al., 2019). Therefore, we quantify the discrepancy between the solution of the
299 heterogeneous three-species model and the homogeneous single-species model
300 using an error measure, $E(\delta)$, associated with the position of the leading edge,

$$E(\delta) = \frac{1}{\alpha} \sum_j \left[\mathcal{S}(t_j) - S(t_j) \right]^2, \quad (4.1)$$

301 where $\mathcal{S}(t_j)$ is the position of the leading edge according to the three-species
302 heterogeneous model at time t_j , $S(t_j)$ is the position of the leading edge pre-
303 dicted by the single-species homogeneous model, and α is a number of discrete
304 time points that we used to compute $E(\delta)$. In both scenarios the position of
305 the leading edge is computed as the coordinate on the one-dimensional domain
306 where the density is 1% of the initial density (Treloar and Simpson, 2013).

307 In the first set of results we present, called Set I, we choose to fix D and f_0 , and
308 vary δ between each subpopulation in the three-species heterogeneous model.
309 The experimental distribution of cell sizes in Figure 1(d) provides insights into
310 potential choices of the cell size distribution in Equations (3.2)-(3.4). Here we
311 define three subpopulations based on the equivalent cell size: small ($18 \mu\text{m}$),
312 medium ($34 \mu\text{m}$), and large cells ($50 \mu\text{m}$). For simplicity, we set the fractions of
313 small and medium cells to be equal and refer to this distribution as a monoton-
314 ically decreasing distribution of cell sizes (Set Ia, Figure 3). After considering
315 the experimentally-motivated monotonically decreasing distribution, we then

316 systematically explore: (i) uniform (Set Ib, Figure 4), (ii) non-monotonic (Set
317 Ic, Figure 5), and (iii) monotonically increasing distributions (Set Id, Figure
318 6).

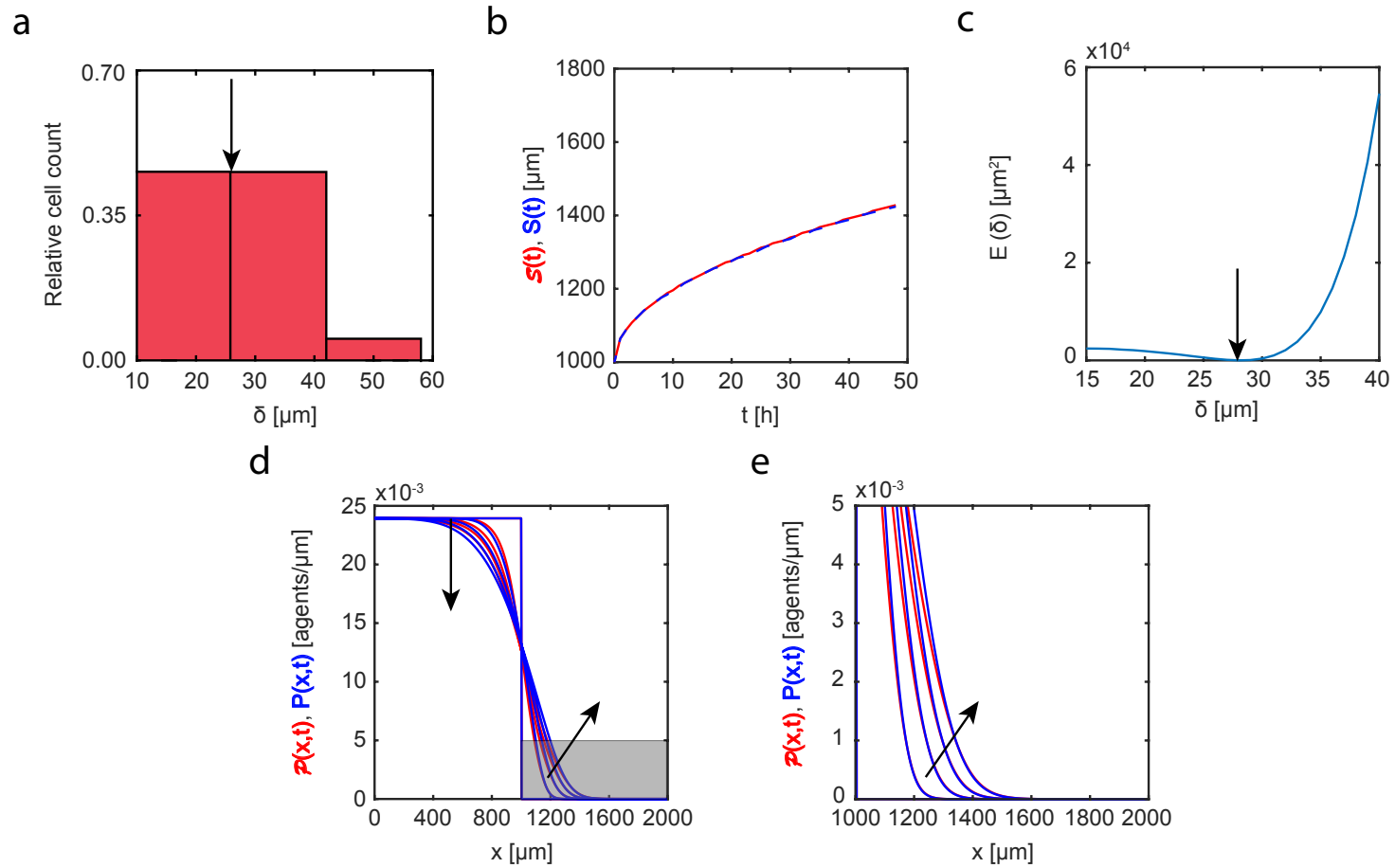


Fig. 3. Set Ia. Heterogeneity in cell sizes: monotonically decreasing distribution. (a) Cell size distribution adopted in the three-species heterogeneous model, Equations (3.2)-(3.4). (b) Leading edge as predicted by the three-species heterogeneous model, $S(t)$ (solid red), and the best-fit approximation given by the single-species homogeneous model, $S(t)$ (blue dashed). (c) Error measure, $E(\delta)$, between the density profiles given by the three-species heterogeneous model and the profiles predicted by the single-species homogeneous model as a function of cell size, δ . The black arrow denotes the best-fit value of cell size, $\delta = 28 \mu\text{m}$. (d)-(e) Cell density profiles predicted by the three-species heterogeneous model, $\mathcal{P}(x,t)$ (solid red), superimposed with density profiles given by the single-species homogeneous model calibrated with the best-fit value of δ , $P(x,t)$ (solid blue). The continuum results for both models are presented at $t = 0, 12, 24, 36,$ and 48 h. Black arrows denote the direction of increasing time. Results in (e) show a close-up comparison right near the leading edge, denoted by the gray shaded region in (d).

319 Figure 3(b) compares the leading edge prediction, $\mathcal{S}(t)$, given by the three-
320 species heterogeneous model with the associated best-fit match, $S(t)$, pre-
321 dicted by the single-species homogeneous model. Our systematic computation
322 of the error measure, $E(\delta)$, demonstrates a clear minimum which ensures the
323 unique choice of a best-fit cell size, δ . Results in Figure 3(d) superimposes
324 the solution of the three-species heterogeneous model with the solution of the
325 single-species homogeneous model parameterised with the best fit cell size.
326 Comparing the time evolution of the spreading density profiles in Figure 3(d)
327 (with additional details at the leading edge shown in the magnified region in
328 Figure 3(e)) we see that the appropriately parameterised single-species homo-
329 geneous model captures the temporal evolution of the spreading profile given
330 by the heterogeneous model remarkably accurately. In particular, the den-
331 sity profiles predicted by the single-species homogeneous model match both
332 the position and shape of the density profiles generated by the three-species
333 heterogeneous model. These results imply that in this case it would be rea-
334 sonable to use a much simpler single-species homogeneous model to describe
335 and predict this spatial spreading.

336 Visual inspection of the results in Figures 3 - 6 suggests that we can always
337 find a unique, well-defined value of the cell size in the single-species homo-
338 geneous model to provide an accurate prediction of the temporal evolution of
339 the position of a leading edge of the spreading heterogeneous cell populations
340 regardless of the underlying cell size distribution in the three-species hetero-
341 geneous model (Figures 3(b)-6(b)). In contrast, the quality of match between
342 the shape of the shape of the density profiles for the three-species hetero-
343 geneous model and the single-species homogeneous model varies significantly
344 between different cell size distributions. For example, the experimentally mo-

345 tivated distribution in Figure 3(a) leads to a remarkably good match between
346 the three-species heterogeneous model and the single-species homogeneous
347 model. In contrast, the shape of the density profiles associated with the non-
348 monotonic cell size distribution (Figure 5) and monotonically increasing cell
349 size distribution (Figure 6) show a relatively poor match. In these cases, it
350 would seem prudent not to use a simpler single-species homogeneous model
351 to simulate and predict these experiments.

352 The values of the cell size, δ , that produce best match between the single-
353 species homogeneous and three-species heterogeneous models vary significantly
354 between different cell size distributions. For example, the best-fit value of the
355 cell size for the uniform distribution (Figure 4), $\delta = 36 \mu\text{m}$, is quite close
356 to the weighted average value of $\delta = 34 \mu\text{m}$ for the distribution in Figure
357 4(a). This indicates that the choice of a simple weighted average of the cell
358 sizes might be a reasonable way to parameterise the single-species homo-
359 geneous model if the experimentally observed distribution is close to uniform.
360 We observe similar agreement for best-fit values of the cell size in the case
361 of monotonically decreasing and monotonically increasing cell size distribu-
362 tions (Figure 3, Figure 6). In contrast, the best-fit value of cell size for the
363 non-monotonic distribution, $\delta = 40 \mu\text{m}$, differs significantly from the weighted
364 average of $\delta = 34 \mu\text{m}$. Therefore, these results suggest that great care out to
365 be exercised when taking a distribution of parameter values and attempting
366 to select the most appropriate single representative value of that parameter.

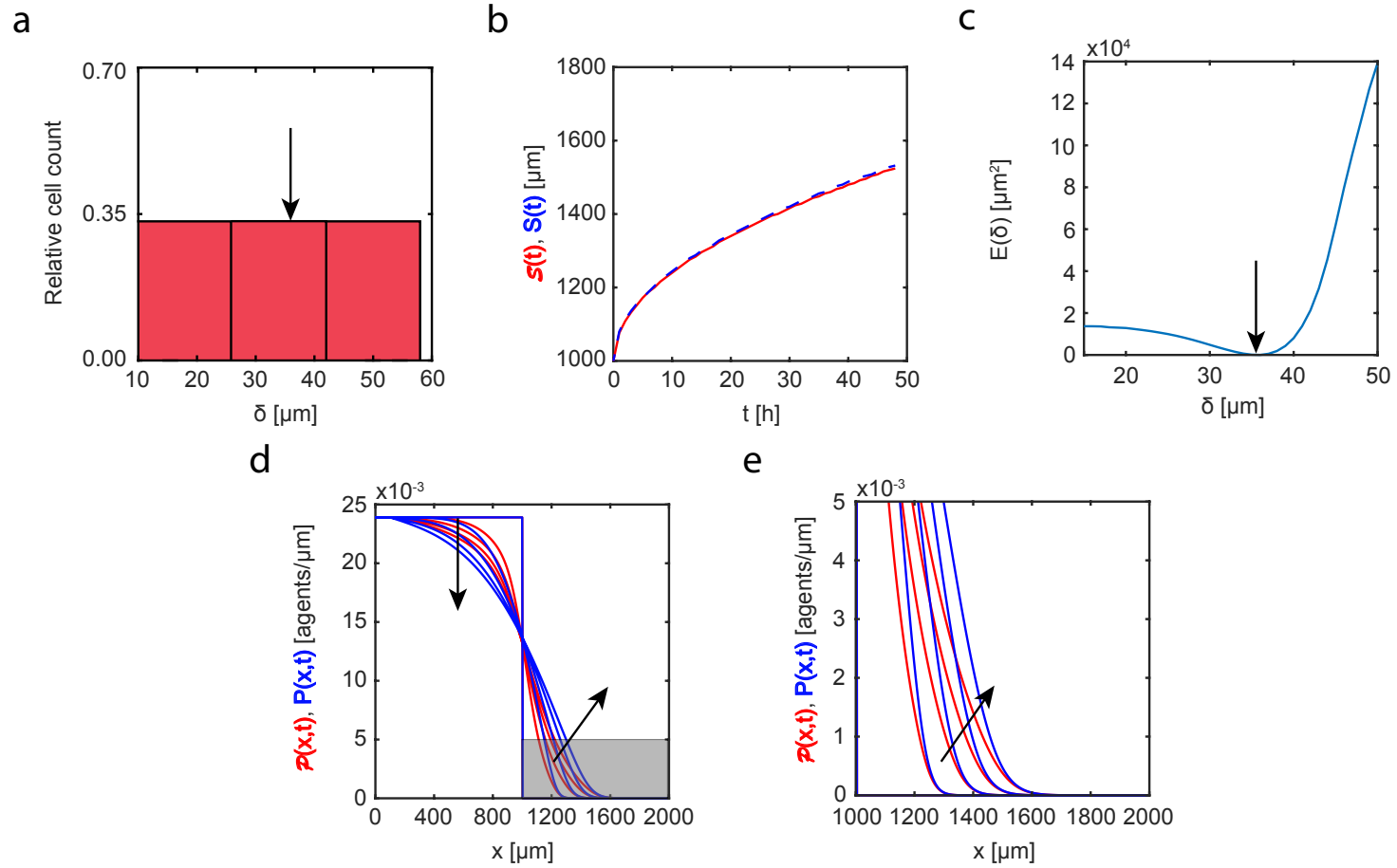


Fig. 4. Set Ib. Heterogeneity in cell sizes: uniform distribution. (a) Cell size distribution adopted in the three-species heterogeneous model, Equations (3.2)-(3.4). (b) Leading edge as predicted by the three-species heterogeneous model, $\mathcal{S}(t)$ (solid red), and the best-fit approximation given by the single-species homogeneous model, $S(t)$ (blue dashed). (c) Error measure, $E(\delta)$, between the density profiles given by the three-species heterogeneous model and the profiles predicted by the single-species homogeneous model as a function of cell size, δ . The black arrow denotes the best-fit value of cell size, $\delta = 36 \mu\text{m}$. (d)-(e) Cell density profiles predicted by the three-species heterogeneous model, $\mathcal{P}(x, t)$ (solid red), superimposed with density profiles given by the single-species homogeneous model calibrated with the best-fit value of δ , $P(x, t)$ (solid blue). The continuum results for both models are presented at $t = 0, 12, 24, 36,$ and 48 h. Black arrows denote the direction of increasing time. Results in (e) show a close-up comparison right near the leading edge, denoted by the gray shaded region in (d).

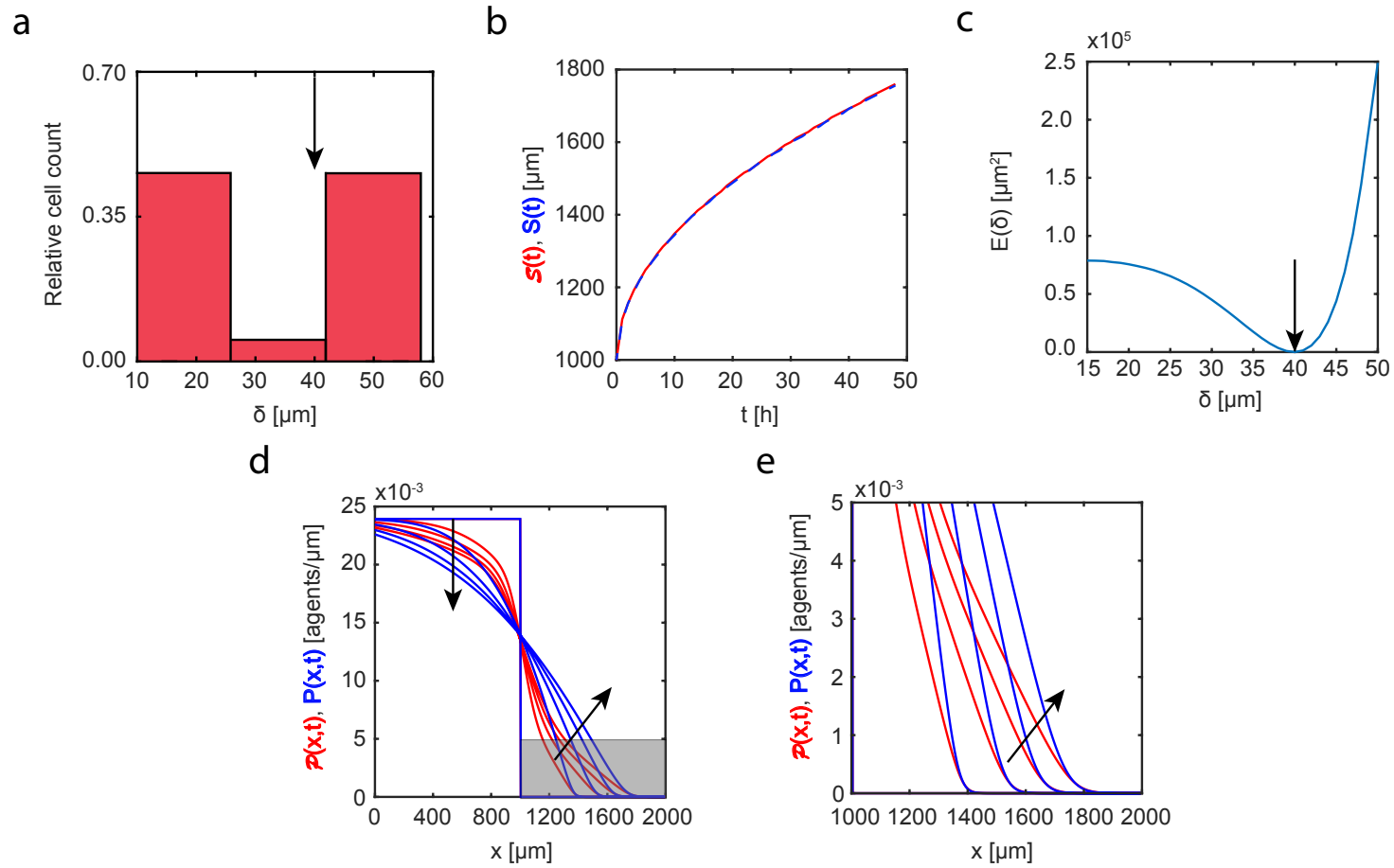


Fig. 5. Set Ic. Heterogeneity in cell sizes: non-monotonic distribution. (a) Cell size distribution adopted in the three-species heterogeneous model, Equations (3.2)-(3.4). (b) Leading edge as predicted by the three-species heterogeneous model, $\mathcal{S}(t)$ (solid red), and the best-fit approximation given by the single-species homogeneous model, $S(t)$ (blue dashed). (c) Error measure, $E(\delta)$, between the density profiles given by the three-species heterogeneous model and the profiles predicted by the single-species homogeneous model as a function of cell size, δ . The black arrow denotes the best-fit value of cell size, $\delta = 40 \mu\text{m}$. (d)-(e) Cell density profiles predicted by the three-species heterogeneous model, $\mathcal{P}(x,t)$ (solid red), superimposed with density profiles given by the single-species homogeneous model calibrated with the best-fit value of δ , $P(x,t)$ (solid blue). The continuum results for both models are presented at $t = 0, 12, 24, 36,$ and 48 h. Black arrows denote the direction of increasing time. Results in (e) show a close-up comparison right near the leading edge, denoted by the gray shaded region in (d).

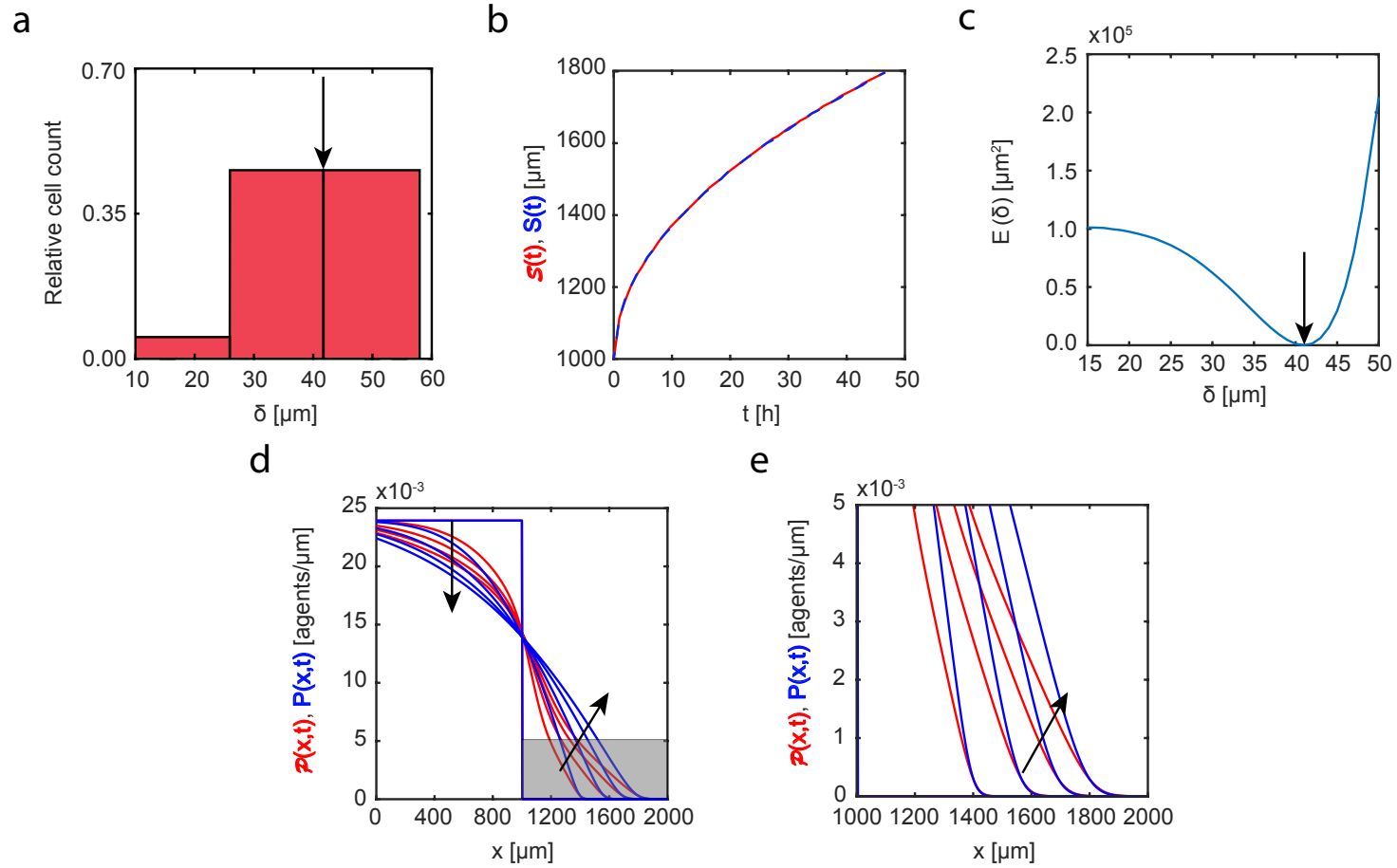


Fig. 6. Set Id. Heterogeneity in cell sizes: monotonically increasing distribution. (a) Cell size distribution adopted in the three-species heterogeneous model, Equations (3.2)-(3.4). (b) Leading edge as predicted by the three-species heterogeneous model, $\mathcal{S}(t)$ (solid red), and the best-fit approximation given by the single-species homogeneous model, $S(t)$ (blue dashed). (c) Error measure, $E(\delta)$, between the density profiles given by the three-species heterogeneous model and profiles predicted by the single-species homogeneous model as a function of cell size, δ . The black arrow denotes the best-fit value of cell size, $\delta = 41 \mu\text{m}$. (d)-(e) Cell density profiles predicted by the three-species heterogeneous model, $\mathcal{P}(x,t)$ (solid red), superimposed with density profiles given by the single-species homogeneous model calibrated with the best-fit value of δ , $P(x,t)$ (solid blue). The continuum results for both models are presented at $t = 0, 12, 24, 36,$ and 48 h. Black arrows denote the direction of increasing time. Results in (e) show a close-up comparison right near the leading edge, denoted by the gray shaded region in (d).

367 In addition to the results in Figures 3 - 6 exploring the role of heterogeneity
368 in cell size, we present an additional suite of results where we systematically
369 explore the role of heterogeneity in D (Set II) and f_0 (Set III) while keeping
370 δ constant. These additional results are presented in the Supplementary Ma-
371 terial document. Both Set II and Set III data sets demonstrate exceptional
372 quality of match between the three-species heterogeneous simulation data and
373 its best-fit single-species homogeneous equivalent. Again, these additional re-
374 sults provide guidance about when it is reasonable to approximate a more
375 complicated heterogeneous mathematical model with a simpler single-species
376 homogeneous model.

377 5 Conclusions

378 In this work, we explore the role of heterogeneity in the context of study-
379 ing how an initially confined population of cells can spread into surround-
380 ing initially unoccupied regions, as in the case of a scratch assay. We use
381 a three-species heterogeneous model of cell motility, account for undirected
382 cell motility, short range repulsion (crowding) and longer range adhesion, to
383 capture experimentally observed heterogeneity in cell sizes from a new exper-
384 imental data set from a two-dimensional scratch assay as shown in Figure 1.
385 Our continuum models account for the undirected random motility, cell-to-cell
386 adhesion, and cell crowding. The single-species homogeneous model is applied
387 to each set of three-species heterogeneous simulation data in an attempt to
388 match cell density profiles.

389 To analyse the performance of the single-species homogeneous model to cap-
390 ture data from our three-species heterogeneous model we consider four dif-

391 ferent cell size distributions: (i) monotonically decreasing distribution, (ii)
392 uniform distribution, (iii) non-monotonic distribution, and (iv) monotonically
393 increasing distribution. Overall, for a set of experimentally-motivated parame-
394 ter combinations, we find that the standard single-species homogeneous model
395 is able to accurately predict the position of the leading edge for all case studies
396 presented. However, the quality of the match between the shape of the density
397 profiles varies significantly depending on the details of the form of the hetero-
398 geneity present. For example, the monotonically decreasing distribution (Set
399 Ia) demonstrates remarkable goodness of fit between the two sets of density
400 profiles, as shown in Figure 3(d). This result is important because the mono-
401 tonically decreasing cell size distribution is chosen to mimic the distribution
402 of the cell sizes observed in our new experimental data set, shown in Figure 1.
403 Similarly, the homogeneous distribution, Figure 4, shows that single-species
404 homogeneous model is able to accurately replicate the three-species heteroge-
405 neous model results. This is an expected result because the uniform population
406 of cells does not involve any heterogeneity and so we might anticipate that
407 the simpler homogeneous model would perform well in this case. In contrast,
408 the single-species homogeneous model does not perform so well when applied
409 to both non-monotonic and monotonically increasing distributions in Figures
410 5-6, respectively. Additionally we explore potential heterogeneity in diffusivity
411 and amplitude of the cell-to-cell interactions (Supplementary material). Over-
412 all, our results suggest that for certain cell size distributions, a simple and
413 computationally efficient single-species homogeneous model is preferable over
414 a three-species heterogeneous model.

415 There are number of ways this work can be extended which we leave for future
416 analysis. All our simulations and analysis focus on treating the heterogeneity

417 in the population of cells by considering the total population to be composed
418 of three distinct subpopulations. For more extreme forms for heterogeneity,
419 such as multi-modal distributions, the results presented in this work could be
420 extended by considering additional subpopulations. Another avenue for further
421 exploration would be to consider heterogeneity in more than one parameter at
422 a time, whereas in this work we have taken the most fundamental approach and
423 examined heterogeneity in just one parameter in isolation from the others. For
424 both of these extensions, the modelling framework presented in this study can
425 be extended to explore these additional features, and we leave such extensions
426 for future consideration. Another option for extending the work would be to
427 consider further details in the mathematical models, such as the effects of
428 combined cell migration and combined cell proliferation. Here we have not
429 pursued this approach because our experimental data set has been carefully
430 prepared to exclude the effects of proliferation so that we can focus just on
431 cell migration and heterogeneity in cell migration alone.

432 **Acknowledgements**

433 This work is supported by the Australian Research Council (DP170100474).
434 Computational resources are provided by the High Performance Computing
435 and Research Support Group at QUT. REB is a Royal Society Wolfson Re-
436 search Merit Award holder, would like to thank the Leverhulme Trust for a
437 Research Fellowship and also acknowledges the BBSRC for funding via grant
438 no. BB/R000816/1.

439 **References**

- 440 [1] Altschuler, S.J., Wu, L.F., 2010. Cellular heterogeneity: when do differences make
441 a difference? *Cell* 141(4), 559-563.
- 442 [2] An, F.-Q., Matsuda, M., Fujii, H., Tang, R.-F., Amemiya, H., Dai, Y.-M.,
443 Matsumoto Y., 2001. Tumor heterogeneity in small hepatocellular carcinoma:
444 Analysis of tumor cell proliferation, expression and mutation of p53 and β -
445 Catenin. *International Journal of Cancer* 93, 468-474.
- 446 [3] Baker, R.E., Simpson, M.J., 2010. Correcting mean-field approximations for
447 birth-death-movement processes. *Physical Review E* 82, 041905.
- 448 [4] Binder, B.J., Simpson, M.J., 2016. Cell density and cell size dynamics during
449 *in vitro* tissue growth experiments: Implications for mathematical models of
450 collective cell behaviour. *Applied Mathematical Modelling* 40, 3438-3446.
- 451 [5] Bobadilla, A.V.P., Arevalo, J., Sarro, E., Byrne, H.M., Maini, P.K., Carraro, T.,
452 Balocco, S., Meseguer, A., Alarcon, T., 2019. In vitro cell migration quantification
453 method for scratch assays. *Journal of the Royal Society Interface* 16, 20180709.
- 454 [6] Cai, A.Q., Landman, K.A., Hughes, B.D., 2007. Multi-scale modeling of a wound-
455 healing cell migration assay. *Journal of Theoretical Biology* 245(3), 576-594.
- 456 [7] Callaghan, T., Khain, E., Sander, L.M., Ziff, R.M., 2006. A stochastic model for
457 wound healing. *Journal of Statistical Physics* 122(5), 909-924.
- 458 [8] Edmondson, R., Broglie, J.J., Adcock, A.F., Yang, L., 2014. Three-dimensional
459 cell culture systems and their applications in drug discovery and cell-based
460 biosensors. *ASSAY and Drug Development Technologies* 12(4), 207-218.
- 461 [9] Essen BioScience: IncuCyte ZOOM live cell imaging.
462 Available from: <http://www.essenbioscience.com/essen-products/incucyte/>
463 (Accessed: May 2019).

- 464 [10] Frascoli, F., Hughes, B.D., Zaman, M.H., Landman, K.A., 2013. A
465 computational model for collective cellular motion in three dimensions: General
466 framework and case study for cell pair dynamics. PLoS ONE 8(3), e59249.
- 467 [11] Galle, J., Loeffler, M., Drasdo D., 2005. Modeling the effect of deregulated
468 proliferation and apoptosis on the growth dynamics of epithelial cell populations
469 *in vitro*. Biophysical Journal 88, 62-75.
- 470 [12] Gerlee, P., 2013. The model muddle: In search of tumor growth laws. Cancer
471 Research 73(8), 2407-2411.
- 472 [13] George, M., Bullo F., Campas O., 2017. Connecting individual to collective cell
473 migration. Scientific Reports 7, 9720.
- 474 [14] Hasenauer, J., Waldherr, S., Doszczak, M., Scheurich, P., Radde, N., Allgwer,
475 F. 2011. Analysis of heterogeneous cell populations: A density-based modeling
476 and identification framework. Journal of Process Control 21, 1417-1425.
- 477 [15] Jeon J, Quaranta V, Cummings PT (2010). An off-lattice hybrid discrete-
478 continuum model of tumor growth and invasion. Biophysical Journal 98 (1): 37-47.
- 479 [16] Jin, W., Shah, E.T., Penington, C.J., McCue, S.W., Chopin, L.K., Simpson,
480 M.J., 2016. Reproducibility of scratch assays is affected by the initial degree of
481 confluence: Experiments, modelling and model selection. Journal of Theoretical
482 Biology 390, 136-145.
- 483 [17] Jin, W., McCue, S.W., Simpson, M.J., 2018. Extended logistic growth model
484 for heterogeneous populations. Journal of Theoretical Biology 445, 51-61.
- 485 [18] Johnston, S.T., Simpson, M.J., McElwain, D.L.S., 2014. How much information
486 can be obtained from tracking the position of the leading edge in a scratch assay?
487 Journal of the Royal Society Interface 11, 20140325.
- 488 [19] Kaighn, M.E., Narayan, K.S., Ohnuki, Y., Lechner, J.F., Jones, L.W., 1979.

- 489 Establishment and characterization of a human prostatic carcinoma cell line (PC-
490 3). *Investigative urology* 17(1), 16-23.
- 491 [20] Maini, P.K., McElwain, D.L.S., Leavesley, D., 2004. Travelling waves in a wound
492 healing assay. *Applied Mathematics Letters* 17(5), 575-580.
- 493 [21] Maini, P.K., McElwain, D.L.S., Leavesley, D., 2004. Traveling wave model to
494 interpret a wound-healing cell migration assay for human peritoneal mesothelial
495 cells. *Tissue Engineering* 10(3/4), 475-482.
- 496 [22] Matsiaka, O.M., Penington, C.J., Baker, R.E., Simpson, M.J., 2017. Continuum
497 approximations for lattice-free multi-species models of collective cell migration.
498 *Journal of Theoretical Biology* 422, 1-11.
- 499 [23] Matsiaka, O.M., Penington, C.J., Baker, R.E., Simpson, M.J., 2018. Discrete
500 and continuum approximations for collective cell migration in a scratch assay with
501 cell size dynamics. *Bulletin of Mathematical Biology* 80(4), 738-757.
- 502 [24] Matsiaka, O.M., Baker, R.E., Simpson, M.J., 2019. Mechanistic and
503 experimental models of cell migration reveal the importance of intercellular
504 interactions in cell invasion. *Biomedical Physics and Engineering Express*. In press
505 [https://doi.org/ 10.1088/2057- 1976/ab1b01](https://doi.org/10.1088/2057-1976/ab1b01).
- 506 [25] Middleton, A.M., Fleck, C., Grima, R., 2014. A continuum approximation to
507 an off-lattice individual-cell based model of cell migration and adhesion. *Journal*
508 *of Theoretical Biology* 359, 220-232.
- 509 [26] Murray, P.J., Edwards, C.M., Tindall, M.J., Maini, P.K., 2009. From a discrete
510 to a continuum model of cell dynamics in one dimension. *Physical Review E* 80(3),
511 031912.
- 512 [27] Nardini, J.T., Chapnick, D.A., Liu, X., Bortz, D.M., 2016 Modeling keratinocyte
513 wound healing dynamics: Cell-cell adhesion promotes sustained collective
514 migration. *Journal of Theoretical Biology* 400, 103-117.

- 515 [28] Newman, T.J., Grima, R., 2004. Many-body theory of chemotactic cell-cell
516 interactions. *Physical Review E* 70, 051916.
- 517 [29] O’Dea, R.D., King, J.R., 2012. Continuum limits of pattern formation in
518 hexagonal-cell monolayers. *Journal of Mathematical Biology* 64, 579-610.
- 519 [30] Osborne, J.M., Fletcher, A.G., Pitt-Francis, J.M., Maini, P.K., Gavaghan, D.J.,
520 2017. Comparing individual-based approaches to modelling the self-organization
521 of multicellular tissues. *PLOS Computational Biology* 13(2), e1005387.
- 522 [31] Painter, K.J., Sherratt, J.A., 2003. Modelling the movement of interacting cell
523 populations. *Journal of Theoretical Biology* 225(3), 327-339.
- 524 [32] Pozzobon, V., Perre, P., 2018. Han’s model parameters for microalgae grown
525 under intermittent illumination: Determined using particle swarm optimization.
526 *Journal of Theoretical Biology* 437, 29-35.
- 527 [33] Sadeghi, H.M., Seitz, B., Hayashi, S., LaBree, L., McDonnell, P.J., 1998. In
528 vitro effects of Mitomycin-C on human keratocytes. *Journal of Refractive Surgery*
529 14, 534-40.
- 530 [34] Sarapata, E.A., de Pillis, L.G., 2010. A comparison and catalog of intrinsic
531 tumor growth models. *Bulletin of Mathematical Biology* 76, 2010-2024.
- 532 [35] Savla, U., Olson, L.E., Waters, C.M., 2004. Mathematical modeling of airway
533 epithelial wound closure during cyclic mechanical strain. *Journal of Applied*
534 *Physiology* 96, 566-574.
- 535 [36] Sengers, B.A., Please, C.P., Oreffo, R.O.C., 2007. Experimental characterization
536 and computational modelling of two-dimensional cell spreading for skeletal
537 regeneration. *Journal of the Royal Society Interface* 4, 1107-1117.
- 538 [37] Sepulveda, N., Petitjean, L., Cochet, O., Grasland-Mongrain, E., Silberzan, P.,
539 Hakim, V., 2016. Collective cell motion in an epithelial sheet can be quantitatively

540 described by a stochastic interacting particle model. PLOS Computational Biology
541 9(3), e1002944

542 [38] Shah, E.T., Upadhyaya, A., Philp, L.K., Tang, T., Skalamera, D., Gunter,
543 J., Nelson, C.C., Williams, E.D., Hollier, B.G., 2016. Repositioning “old” drugs
544 for new causes: identifying new inhibitors of prostate cancer cell migration and
545 invasion. *Clinical & Experimental Metastasis* 33, 385-399.

546 [39] Sheardown, H., Cheng, Y.-L., 1995. Mechanisms of corneal epithelial wound
547 healing. *Chemical Engineering Science* 51(19), 4517-4529.

548 [40] Sherratt, J.A., Murray, J.D., 1990. Models of epidermal wound healing.
549 *Proceedings of the Royal Society B* 241, 29-36.

550 [41] Sundstrom, A., Bar-Sagi, D., Mishra, B., 2016. Simulating heterogeneous tumor
551 cell populations. *PLoS ONE* 11(12), e0168984.

552 [42] Simpson, M.J., Treloar, K.K., Binder, B.J., Haridas, P., Manton, K.J.,
553 Leavesley, D.I., McElwain, D.L.S., Baker, R.E., 2013. Quantifying the roles of
554 cell motility and cell proliferation in a circular barrier assay. *Journal of the Royal*
555 *Society Interface* 10, 20130007.

556 [43] Simpson, M.J., Haridas P., McElwain D.L.S., 2014. Do pioneer cells exist? *PLoS*
557 *ONE* 9(1), e85488.

558 [44] Simpson M.J., Jin, W., Vittadello, S.T., Tambyah, T.A., Ryan, J.M.,
559 Gunasingh, G., Haass, N.K., McCue, S.W., 2018. Stochastic models of cell invasion
560 with fluorescent cell cycle indicators. *Physica A* 510, 375-386.

561 [45] Tersoff, J., 1988. New empirical approach for the structure and energy of
562 covalent systems. *Physical Review B* 37(12), 6991-7000.

563 [46] ThermoFisher Scientific. Available from:
564 <https://www.thermofisher.com/au/en/home/life-science/cell->

565 culture/mammalian-cell-culture/reagents/trypsin/tryple-express.html (Accessed:
566 May, 2019).

567 [47] Treloar, K.K., Simpson, M.J. 2013. Sensitivity of edge detection methods for
568 quantifying cell migration assays. PLoS ONE 8(6), e67389.

569 [48] Tremel, A., Cai, A., Tirtaatmadja, N., Hughes, B.D., Stevens, G.W., Landman,
570 K.A., O'Connor, A.J., 2009. Cell migration and proliferation during monolayer
571 formation and wound healing. Chemical Engineering Science 64, 247-253.

572 [49] Warne, D.J., Baker, R.E., Simpson, M.J., 2019. Simulation and inference
573 algorithms for stochastic biochemical reaction networks: from basic concepts to
574 state-of-the-art. Journal of the Royal Society Interface 16, 20180943.

575 [50] Wise, S.M., Lowengrub, J.S., Frieboes, H.B., Cristini, V., 2008. Three-
576 dimensional multispecies nonlinear tumor growth—I Model and numerical method.
577 Journal of Theoretical Biology 253(3), 524-543.